Synthesis of phosphonic acid ligands for nanocrystal surface functionalization and solution processed memristors

Jonathan De Roo,[1,2*] Zimu Zhou,[3] Jiaying Wang,[3] Loren Deblock,[1] Alfred J. Crosby,[4] Jonathan S. Owen[2], Stephen S. Nonnenmann[3*]

[1] Department of Chemistry, Ghent University, Gent B-9000, Belgium

[2] Department of Chemistry, Columbia University, New York, NY 10027, USA

[3] Department of Mechanical and Industrial Engineering, University of Massachusetts-Amherst, Amherst, MA 01003, USA

[4] Polymer Science and Engineering Department, University of Massachusetts-Amherst, Amherst, Massachusetts 01003, USA

* Corresponding authors:

Jonathan De Roo, Jonathan.DeRoo@ugent.be

Stephen S. Nonnenmann, ssn@umass.edu

Abstract

Here we synthesize 2-ethylhexyl, 2-hexyldecyl, 2-[2-(2-methoxyethoxy)ethoxy]ethyl, oleyl and *n*-octadecyl phosphonic acid and use them to functionalize CdSe and HfO_2 nanocrystals. In contrast to branched carboxylic acids, post-synthetic surface functionalization of CdSe and HfO_2 nanocrystals is readily achieved with branched phosphonic acids. Phosphonic acid capped HfO_2 nanocrystals are subsequently evaluated as memristor using conductive atomic force microscopy (c-AFM). We find that 2-ethylhexyl phosphonic acid is a superior ligand, combining a high colloidal stability with a compact ligand shell that results in a record-low operating voltage that is promising for application in flexible electronics.

Introduction

Surface engineering of colloidal nanocrystals (NCs) is a prerequisite for advanced applications such as solar cells,[1,2] thermoelectrics,[3] field effect transistors,[4] smart windows,[5] superconductors,[6,7] catalysis[8] and memristors.[9] In particular, threshold memristors garner intense research interest because they emulate synaptic responses in neuromorphic computing.[10] They also exhibit faster switching speeds, lower power consumption, higher scalability, and greater 3D stackability than standard complementary metal oxide semiconductor (CMOS) circuits, thus promoting further miniaturizing beyond Moore's Law.[11,12] In such threshold switching, a bias is applied, resulting in current flow and a significant amount of internal Joule heating. Once above the metal-insulator transition,[13] the device is activated and maintains a low resistance state (LRS) until the voltage is removed and the device resets to an insulating high resistance state (HRS). A memristor device comprises an insulating oxide layer sandwiched between two metal electrodes, typically fabricated by a vacuum deposition processes. However, these conventional approaches are limited due to expensive fabrication equipment and small deposition areas.[14] A facile and cost effective

alternative is the solution deposition of monodisperse, highly crystalline inorganic NCs (e.g., $SrTiO_3$, HfO_2) into ribbons of nanocrystals via evaporative assembly using flow coating.[9, 15, 16] In addition, conductive atomic force microscopy (c-AFM) has the ability to locally interrogate electrical properties across length scales (a few nm – 100 μm) relevant to both individual NCs and the nanoribbon assemblies. Therefore, we have used c-AFM analysis to show that operating parameters such as set/reset voltage and LRS/HRS ratios of the nanoribbons inversely scale with the length of the ligand used to stabilize the NCs in solution.[9] Therefore, short ligands are desired but ligands shorter than dodecanoic acid result in unstable dispersions, thereby restraining the minimum set voltage that could be used to switch the ribbons of NCs.

With respect to ligands, the oleyl fragment is ubiquitous in the nanocrystal field; many syntheses utilize either oleylamine or oleic acid as the surfactant.[17-20] The unsaturation provides a high dispersibility in organic solvents and offers a distinct signal in liquids ^{1}H nuclear magnetic resonance (NMR) spectroscopy. The latter is especially appealing for surface chemistry studies because liquids NMR spectroscopy is the method of choice for monitoring ligand binding and exchange on colloidal NCs.[21, 22] Peng and coworkers recently showed that NCs with short, branched ligands are more dispersible than NCs with long, straight chain ligands.[23] They used 2-ethylhexanethiol as a champion ligand to obtain high conductance in solution processed thin films of CdSe NCs. Thiols bind well to CdSe and metal NCs but they are poor ligands for metal oxides. Whereas carboxylic acids have a reasonably high affinity for metal oxides,[24, 25] exchange of native oleate ligands for 2-hexyldecanoic acid proved to be unfavorable because of the steric encumbrance of the branched aliphatic chain.[26] Interestingly, phosphonic acid ligands are known to quantitatively displace carboxylate ligands on CdSe,[27, 28] PbSe,[29] and ZrO_2[30] NCs and also bind well to flat surfaces.[25, 31] Saturated phosphonic acids are also used in the synthesis of wurtzite CdSe NCs.[32-34] However, post-synthetic functionalization

of NCs still mostly focuses on carboxylic acid or thiol ligands, even though the latter typically quench the photoluminescence quantum yield.[35, 36]

Here, we explore the functionalization of NCs with phosphonic acid derivatives **1** – **5** (Scheme 1) and their fabrication into memristor devices. We selected novel, branched phosphonic acids (**1** and **2**), a versatile polyethylene glycol[34, 37-40] derivative (**3**), as yet unreported oleylphosphonic acid (**4**) and a prototypical straight chain derivative (**5**). The convenient synthesis of these phosphonic acids is followed by surface functionalization methods that are facile, even for the branched substrates. Finally, using this ligands, we deposit HfO_2 NCs into ribbons of NCs by a simple flow coating process and measure their local memristive current-voltage response with c-AFM.

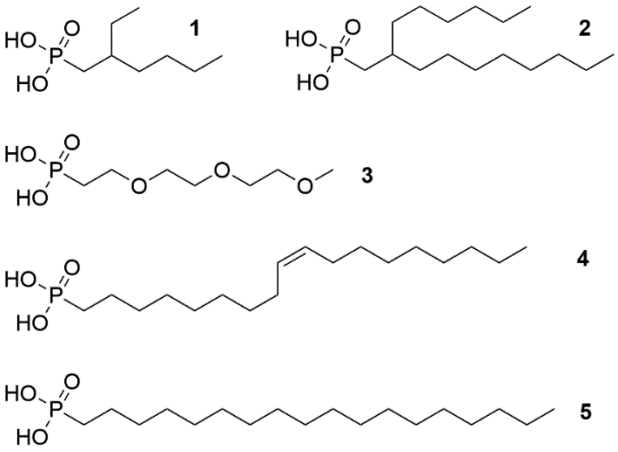

Scheme 1. Target phosphonic acid ligands, tailored towards nanocrystal surfaces.

Results and discussion

Phosphonic acids are usually synthesized via the Michaelis-Arbuzov reaction (Scheme 2).[41, 42] High temperatures (160 °C) are often required and generally, only primary, sterically unencumbered halides react (thus not suitable for target compounds **1** and **2**).[43] The scope is also limited by side reactions with an ethyl bromide coproduct that leads to ethyl phosphonate

ester byproducts. Alternative Michaelis-Arbuzov conditions have been developed that address some of these issues, but remain ineffective for sterically congested substrates,[44] or are only suitable for benzylic substrates.[45]

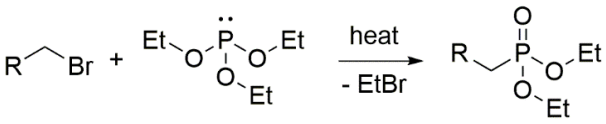

Scheme 2. The Michaelis-Arbuzov reaction.

Faster reactions and lower temperatures are accessible using the Michaelis-Becker approach, wherein a dialkyl phosphite anion is prepared from $CsCO_3$[46] or sodium hydride in THF[47] or Na in hexane[48] in place of the tri-*n*-alkylphosphite as the nucleophile. Following this precedent, we prepared diethyl phosphonate esters from sodium diethylphosphite and the appropriate alkyl bromide in dimethylformamide solution (Scheme 3).[49] Reactions reached completion within a few hours at room temperature for linear alkyl bromides and at 70 ˚C for branched substrates. Only compound **3** could not be synthesized in high purity using the Michaelis-Becker reaction (neither in DMF, nor in THF) due to slow conversion and the formation of various uncharacterized byproducts. In this case the Michaelis-Arbuzov method was used and the ethyl phosphonate ester byproduct was removed from **3** by distillation.

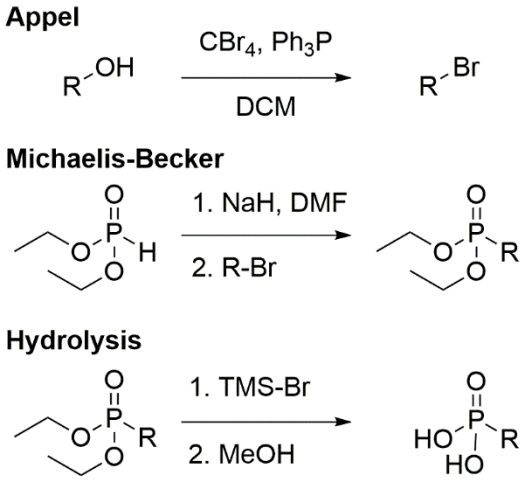

Scheme 3. The Appel reaction converts alcohols in bromides,[50, 51] the Michaelis-Becker reaction converts bromides to phosphonate esters and finally, the phosphonate esters are hydrolyzed to phosphonic acids.

Pure phosphonate ester derivatives **1** – **4** are isolated in greater than 70% yield by distillation, and provided pure samples of phosphonic acid upon treatment with bromotrimethylsilane and methanol (Scheme 3).[52] **5** was purified by recrystallization as the phosphonic acid. Via single crystal diffraction, it was found that **5** crystallizes in the monoclinic crystal structure and forms a stacked arrangement (Figure 1A). The acidic hydrogens form a hydrogen bond to the oxygen lone pairs of the P=O bond with the hydrogen bonds being inequivalent, measuring 1.84 (4) Å and 1.79 (5) Å, (Figure 1B). Compound **4** is a waxy solid and can in principle also be recrystallized from hexane but the yield is low (20 %) and this increases the relative amount of trans-**2** compared to cis-**2**.

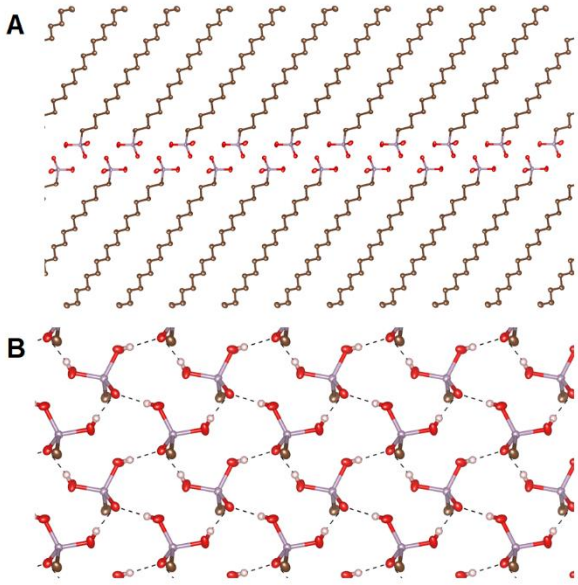

Figure 1. Crystal structure of **5**. (A) View along the [010] direction, hydrogens are omitted for clarity. The aliphatic chains angle towards the reader at an angle of 45°. The chain packing density is 3.3 nm^{-2}. (B) View along the [001] direction, hydrogen bonds are displayed. Only the first carbon of the chain is depicted for clarity.

Next, we demonstrate the versatility of our compounds with respect to nanocrystal surfaces. As a model system, cadmium oleate capped CdSe NCs (d = 3.3 nm, Figure S1) were synthesized according to Cao et al.,[53] and purified by precipitation with methyl acetate (see supporting information for experimental details). Figure 2A shows the characteristically broadened NMR resonances of bound oleate ligands in $CDCl_3$. Although oleate ligands can be quantitatively replaced with linear phosphonic acids,[27, 28] the question remains whether branched phosphonic acids react identically. To investigate this, we added 1.2 equivalents of **1** to the CdSe NCs in $CDCl_3$. Consequently, the alkene resonance narrows and its multiplicity, typical for free, unbound ligands appears (Figure 2A, inset). After purification (see Supporting information), the ^{1}H NMR spectrum only features the broadened resonances of **1** and no trace of oleate is detected (Figure 2B), indicating a successful exchange of oleate for **1**. To further confirm the successful purification, we performed pulsed field gradient experiments. The resulting diffusion decay is fitted with a single exponential (Figure S2), indicating that **1** is mostly bound to the nanocrystal and the amount of free ligand, if any, is small (< 5%). The

diffusion coefficient of bound **1** is 133 µm²/s, much smaller that the diffusion coefficient of free **1**; 550 µm²/s. The bound nature of **1** is further corroborated by a broad ^{31}P NMR resonance at 33 ppm (FWHM = 2000 Hz, Figure 2B, inset). This compares to a line width of only 65 Hz for free phosphonic acid. Following the exchange, the aerial density of surface ligands[54] was unchanged (4.4 ± 0.5 oleates per nm^2 and 4.7 ± 0.5 phosphonates per nm^2). We conclude that a complete one-for-one exchange of oleate for the branched ligand **1** is achieved and they exist as monohydrogenphosphonate ligands when bound to the surface, in line with earlier reports.[27] The complete exchange with **1** is interesting in light of the poor exchange reactivity of 2-hexyldecanoic acid,[26] and suggests that the higher binding affinity of the phosphonate head-group for the surface, overcomes any steric issue associated with the branched chain (note: the branch point is β to the phosphonate center, while it at the α–position in 2-hexyldecanoate).

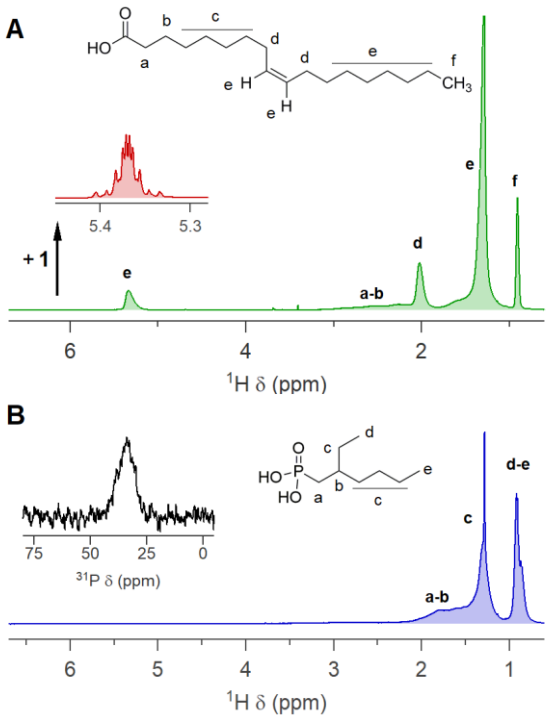

Figure 2. (A) ^{1}H NMR spectrum of oleate capped CdSe nanocrystals in $CDCl_3$ ([NC] = 261 µM, [oleate] = 39 mM). The ligand density is 4.4 ± 0.5 nm^{-2}. The inset shows the alkene resonance after addition of 1.2 equivalents of **1** (B)) ^{1}H NMR spectrum of CdSe nanocrystals in $CDCl_3$, after ligand exchange for **1** and purification. ([NC] = 124 µM, [phosphonate] = 20 mM). The ligand density is 4.7 ± 0.5 nm^{-2}. The inset shows the ^{31}P NMR spectrum.

Using the same exchange strategy, CdSe nanocrystals are readily functionalized with ligands **2 – 5** in chloroform solution. Nanocrystals bound by **1**, **2**, **4** and **5** are dispersible in chloroform, toluene and hexane. As expected, ligand **3** is more versatile and stabilizes NCs in a variety of solvents, including methanol, ethanol, acetone, chloroform and toluene, however, hexane precipitates NCs functionalized with **3** from those solvents.

We utilize ligands **1** – **5** to prepare memristors based on hafnium oxide NCs. HfO_2 NCs (d = 3.75 nm) are synthesized in benzyl alcohol from hafnium(IV) *tert*-butoxide.[55] As-synthesized NCs are not stabilized by ligands and simply washed with diethyl ether to remove organics. Subsequently, the NCs are functionalized by the addition of ligands **1** – **5** and purified (see SI for experimental details). TEM images of these nanoparticles reveal an interparticle distance that varies from 1.6 nm for **1** to 2.4 nm for **5** (Figure 3A-B). The NCs with ligands **1**, **2**, **4** and **5** are well purified by precipitation with methanol, as attested by solution ^{1}H NMR (Figure 3C) and ^{31}P NMR (Figure 3D) so only a monolayer of ligands is attached to the NCs. HfO_2 NCs capped with **3** can only be precipitated using hexane, however, ligand **3** is also insoluble in hexane and is not readily separated from the HfO_2 NCs (Figure 3C and 3D).

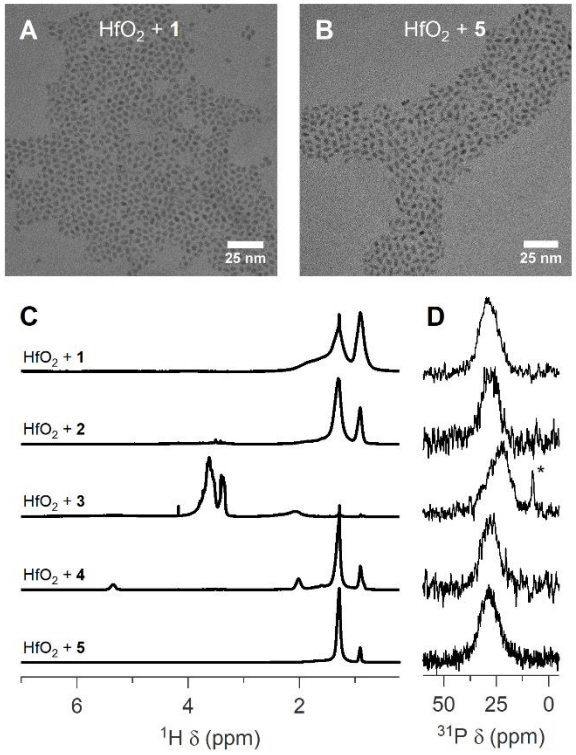

Figure 3. (A) TEM image of HfO_2 NCs functionalized with **1**. (B) TEM image of HfO_2 NCs functionalized with **5**. (C) Solution ^1H NMR and (D) solution ^{31}P NMR spectra of HfO_2 NCs functionalized with **1** – **5** in $CDCl_3$. The resonance with the asterisk is an unidentified impurity.

Thin films of hafnium oxide are typically used as a CMOS-compatible high-κ dielectric gate oxide[56] and in memristor applications.[57] HfO_2 NCs, when assembled into ribbons of nanoparticles, feature a low resistance state and a high resistance state, interesting for resistive random access memory (RRAM) applications.[9, 11, 12] Using a mixture of dodecanoic acid and 10-undecenoic acid as ligands adsorbed on the HfO_2 NCs, we previously achieved a minimal threshold switching set voltage of 1.2 ± 0.3 V.[9] In the same fashion, we assemble here the phosphonic acid capped HfO_2 NCs in ribbons of nanoparticles (Figure S3-S8, see SI for experimental details) and measured the switching properties in function of the ligands **1** – **5** (Figure 4). Use of a conductive scan probe as a top electrode enables measurements of nanoribbons in a geometry similar to the nano-crossbar memristor or atomic switch arrays used

in thin film-based devices,[11,12] where both the bias and current response occur across the nanostack dimension.

Conductive atomic force microscopy (c-AFM) was used in point spectroscopic mode to collect 40 I-V curves over four separate, individual nanoribbons for each ligand type. We observed the expected trend where operating voltage scales with ligand size. Here the set voltage varies from extremely high (4.4 ± 0.7 V) for ligands **4** and **5** to a record low (1.0 ± 0.3 V) for ligand **1**. Also bipolar switching is observed or HfO_2 nanocrystal assemblies with ligand **1** (Figure S9). Note that ligand **3** violates the trend and displays higher set voltages than expected for its ligand length. This may be caused by the presence of the free ligand (which proved difficult to remove from the nanocrystals as described above) or by the nature of the polyethylene glycol chain. Note that the triangular cross-section of the nanoribbons (Figs. S3 – S8) creates a thickness-dependence in the memristive response. The thickest portion of the nanoribbons is difficult to electroform using the ± 10 V bias supply of the microscope, and therefore we performed all conductive probe measurements in thinner areas of equivalent thickness (~ 80 nm, circle marker Fig. S10) for each nanoribbon tested. We anticipate that ribbons a few NCs in height will exhibit optimal switching character.

Since it is desirable to minimize the set voltage for future memory applications, the shortest possible ligand should be used, which is **1** in this case of 3.75 nm HfO_2 NCs. However, larger HfO_2 NCs, such as the 5 nm NCs synthesized from $HfCl_4$ and benzyl alcohol,[24] cannot be stabilized by **1**, and the NCs precipitate after functionalization and purification. This is rationalized by the van der Waals attraction between the cores (Figure S11). In this case, colloidal stability is provided by **2**, which it is still considerably shorter than the standard ligands (such as oleic acid) that are typically used. Together, these results place the branched ligands **1** and **2** squarely in the focus of electronic applications where solution processing is combined with interparticle charge transfer after assembly.

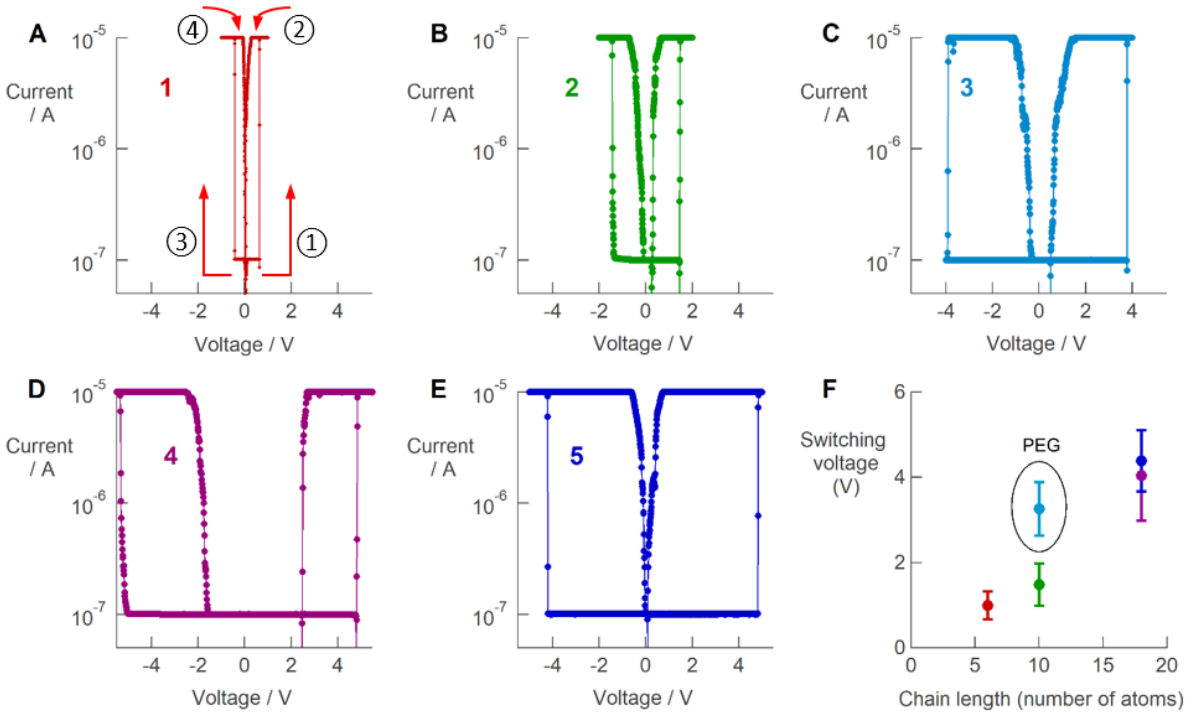

Figure 4. (A) – (E) I-V curve of the threshold switching of HfO_2 nanoribbons using **1 - 5** respectively as ligand. (F) Switching voltage in function of the ligand chain length.

Conclusion

We have developed a scalable synthesis of new phosphonic acid surfactant ligands. We have subsequently shown their superiority in functionalizing nanocrystals surfaces. Whereas exchange for branched carboxylic acids is disfavored by the branching, the branched phosphonic acids readily undergo displacement of the parent carboxylate ligands. Finally, 2-ethylhexyl phosphonic acid leads to a record-low operating voltage in the resistive switching of HfO_2 NC assemblies. Considering their high binding affinity, we expect the synthesized ligands to be heavily used to functionalize surfaces, even beyond the nanocrystal field.

Acknowledgements

The authors thank David A. Sambade for solving the crystal structure of *n*-octadecylphosphonic acid. JDR acknowledges the Belgian American Education Foundation

(B.A.E.F.), Fulbright, Ghent University and the COMPASS project (H2020-MSCA-RISE-2015-691185) for financial support. ZZ, JW and SSN. were partially supported by University of Massachusetts-Amherst start-up funding and the UMass Center for Hierarchical Manufacturing (CHM), and NSF Nanoscale Science and Engineering Center (CMMI-1025020). This work was supported by the U.S. Army Research Laboratory and the U.S. Army Research Office under contract number W911NF-12-1-0594 (MURI).

Associated Content

Supporting information

UV-VIS spectrum of CdSe nanocrystals, DOSY decay fittings, additional NMR spectra, AFM images of nanoribbons, switching results and calculations of the interaction potential. This information is available free of charge via the internet at http://pubs.acs.org/

CCDC 1844778 contains the supplementary crystallographic data for this paper. This data is provided free of charge by The Cambridge Crystallographic Data Centre.

References

1. Sanehira, E. M.; Marshall, A. R.; Christians, J. A.; Harvey, S. P.; Ciesielski, P. N.; Wheeler, L. M.; Schulz, P.; Lin, L. Y.; Beard, M. C.; Luther, J. M., Enhanced mobility CsPbI3 quantum dot arrays for record-efficiency, high-voltage photovoltaic cells. *Sci. Adv.* **2017,** 3, eaao4204.
2. Lan, X.; Voznyy, O.; Garcia de Arquer, F. P.; Liu, M.; Xu, J.; Proppe, A. H.; Walters, G.; Fan, F.; Tan, H.; Yang, Z.; Hoogland, S.; Sargent, E. H., 10.6% Certified Colloidal Quantum Dot Solar Cells via Solvent-Polarity-Engineered Halide Passivation. *Nano Lett.* **2016,** 16, 4630-4634.
3. Ibanez, M.; Luo, Z.; Genc, A.; Piveteau, L.; Ortega, S.; Cadavid, D.; Dobrozhan, O.; Liu, Y.; Nachtegaal, M.; Zebarjadi, M.; Arbiol, J.; Kovalenko, M. V.; Cabot, A., High-performance thermoelectric nanocomposites from nanocrystal building blocks. *Nat. Commun.* **2016,** 7, 10766.
4. Wang, Y.; Fedin, I.; Zhang, H.; Talapin, D. V., Direct optical lithography of functional inorganic nanomaterials. *Science* **2017,** 357, 385-388.
5. Llordes, A.; Garcia, G.; Gazquez, J.; Milliron, D. J., Tunable near-infrared and visible-light transmittance in nanocrystal-in-glass composites. *Nature* **2013,** 500, 323.
6. Rijckaert, H.; Pollefeyt, G.; Sieger, M.; Hanisch, J.; Bennewitz, J.; De Keukeleere, K.; De Roo, J.; Huhne, R.; Backer, M.; Paturi, P.; Huhtinen, H.; Hemgesberg, M.; Van Driessche, I.,

Optimizing Nanocomposites through Nanocrystal Surface Chemistry: Superconducting YBa2Cu3O7 Thin Films via Low-Fluorine Metal Organic Deposition and Preformed Metal Oxide Nanocrystals. *Chem. Mater.* **2017,** 29, 6104-6113.
7. De Keukeleere, K.; Cayado, P.; Meledin, A.; Vallès, F.; De Roo, J.; Rijckaert, H.; Pollefeyt, G.; Bruneel, E.; Palau, A.; Coll, M.; Ricart, S.; Van Tendeloo, G.; Puig, T.; Obradors, X.; Van Driessche, I., Superconducting YBa2Cu3O7-δ Nanocomposites Using Preformed ZrO2 Nanocrystals: Growth Mechanisms and Vortex Pinning Properties. *Adv. Electron. Mater.* **2016,** 2, 1600161.
8. De Roo, J.; Van Driessche, I.; Martins, J. C.; Hens, Z., Colloidal metal oxide nanocrystal catalysis by sustained chemically driven ligand displacement. *Nat. Mater.* **2016,** 15, 517-521.
9. Wang, J.; Choudhary, S.; De Roo, J.; De Keukeleere, K.; Van Driessche, I.; Crosby, A. J.; Nonnenmann, S. S., How Ligands Affect Resistive Switching in Solution-Processed HfO2 Nanoparticle Assemblies. *ACS Appl. Mater. Interfaces* **2018,** 10, 4824-4830.
10. Wang, Z.; Joshi, S.; Savel'ev, S. E.; Jiang, H.; Midya, R.; Lin, P.; Hu, M.; Ge, N.; Strachan, J. P.; Li, Z.; Wu, Q.; Barnell, M.; Li, G.-L.; Xin, H. L.; Williams, R. S.; Xia, Q.; Yang, J. J., Memristors with diffusive dynamics as synaptic emulators for neuromorphic computing. *Nat. Mater.* **2016,** 16, 101.
11. Sawa, A., Resistive switching in transition metal oxides. *Mater. Today* **2008,** 11, 28-36.
12. Waser, R.; Aono, M., Nanoionics-based resistive switching memories. *Nat. Mater.* **2007,** 6, 833.
13. Slesazeck, S.; Mähne, H.; Wylezich, H.; Wachowiak, A.; Radhakrishnan, J.; Ascoli, A.; Tetzlaff, R.; Mikolajick, T., Physical model of threshold switching in NbO2 based memristors. *RSC Adv.* **2015,** 5, 102318-102322.
14. Xu, W.; Li, H.; Xu, J.-B.; Wang, L., Recent Advances of Solution-Processed Metal Oxide Thin-Film Transistors. *ACS Appl. Mater. Interfaces* **2018,** 10, 25878-25901.
15. Kim, H. S.; Lee, C. H.; Sudeep, P. K.; Emrick, T.; Crosby, A. J., Nanoparticle Stripes, Grids, and Ribbons Produced by Flow Coating. *Adv. Mater.* **2010,** 22, 4600-4604.
16. Wang, J.; Choudhary, S.; Harrigan, W. L.; Crosby, A. J.; Kittilstved, K. R.; Nonnenmann, S. S., Transferable Memristive Nanoribbons Comprising Solution-Processed Strontium Titanate Nanocubes. *ACS Appl. Mater. Interfaces* **2017,** 9, 10847-10854.
17. Mourdikoudis, S.; Liz-Marzan, L. M., Oleylamine in Nanoparticle Synthesis. *Chem. Mater.* **2013,** 25, 1465-1476.
18. Sowers, K. L.; Swartz, B.; Krauss, T. D., Chemical Mechanisms of Semiconductor Nanocrystal Synthesis. *Chem. Mater.* **2013,** 25, 1351-1362.
19. Buonsanti, R.; Milliron, D. J., Chemistry of Doped Colloidal Nanocrystals. *Chem. Mater.* **2013,** 25, 1305-1317.
20. Park, J.; Joo, J.; Kwon, S. G.; Jang, Y.; Hyeon, T., Synthesis of monodisperse spherical nanocrystals. *Angew. Chem., Int. Ed.* **2007,** 46, 4630-4660.
21. Marbella, L. E.; Millstone, J. E., NMR Techniques for Noble Metal Nanoparticles. *Chem. Mater.* **2015,** 27, 2721-2739.
22. Hens, Z.; Martins, J. C., A Solution NMR Toolbox for Characterizing the Surface Chemistry of Colloidal Nanocrystals. *Chem. Mater.* **2013,** 25, 1211-1221.
23. Yang, Y.; Qin, H.; Jiang, M.; Lin, L.; Fu, T.; Dai, X.; Zhang, Z.; Niu, Y.; Cao, H.; Jin, Y.; Zhao, F.; Peng, X., Entropic Ligands for Nanocrystals: From Unexpected Solution Properties to Outstanding Processability. *Nano Lett.* **2016,** 16, 2133-2138.

24. De Roo, J.; Van den Broeck, F.; De Keukeleere, K.; Martins, J. C.; Van Driessche, I.; Hens, Z., Unravelling the Surface Chemistry of Metal Oxide Nanocrystals, the Role of Acids and Bases. *J. Am. Chem. Soc.* **2014,** 136, 9650-9657.
25. Pujari, S. P.; Scheres, L.; Marcelis, A. T. M.; Zuilhof, H., Covalent Surface Modification of Oxide Surfaces. *Angew. Chem., Int. Ed.* **2014,** 53, 6322-6356.
26. De Nolf, K.; Cosseddu, S. M.; Jasieniak, J. J.; Drijvers, E.; Martins, J. C.; Infante, I.; Hens, Z., Binding and Packing in Two-Component Colloidal Quantum Dot Ligand Shells: Linear versus Branched Carboxylates. *J. Am. Chem. Soc.* **2017,** 139, 3456-3464.
27. Gomes, R.; Hassinen, A.; Szczygiel, A.; Zhao, Q. A.; Vantomme, A.; Martins, J. C.; Hens, Z., Binding of Phosphonic Acids to CdSe Quantum Dots: A Solution NMR Study. *J. Phys. Chem. Lett.* **2011,** 2, 145-152.
28. Knauf, R. R.; Lennox, J. C.; Dempsey, J. L., Quantifying Ligand Exchange Reactions at CdSe Nanocrystal Surfaces. *Chem. Mater.* **2016,** 28, 4762-4770.
29. Woo, J. Y.; Lee, S.; Kim, W. D.; Lee, K.; Kim, K.; An, H. J.; Lee, D. C.; Jeong, S., Air-Stable PbSe Nanocrystals Passivated by Phosphonic Acids. *J. Am. Chem. Soc.* **2016,** 138, 876-883.
30. De Keukeleere, K.; Coucke, S.; De Canck, E.; Van Der Voort, P.; Delpech, F.; Coppel, Y.; Hens, Z.; Van Driessche, I.; Owen, J. S.; De Roo, J., Stabilization of Colloidal Ti, Zr, and Hf Oxide Nanocrystals by Protonated Tri-n-octylphosphine Oxide (TOPO) and Its Decomposition Products. *Chem. Mater.* **2017,** 29, 10233-10242.
31. Queffélec, C.; Petit, M.; Janvier, P.; Knight, D. A.; Bujoli, B., Surface Modification Using Phosphonic Acids and Esters. *Chem. Rev.* **2012,** 112, 3777-3807.
32. Drijvers, E.; De Roo, J.; Geiregat, P.; Fehér, K.; Hens, Z.; Aubert, T., Revisited Wurtzite CdSe Synthesis: A Gateway for the Versatile Flash Synthesis of Multishell Quantum Dots and Rods. *Chem. Mater.* **2016,** 28, 7311-7323.
33. Carbone, L.; Nobile, C.; De Giorgi, M.; Sala, F. D.; Morello, G.; Pompa, P.; Hytch, M.; Snoeck, E.; Fiore, A.; Franchini, I. R.; Nadasan, M.; Silvestre, A. F.; Chiodo, L.; Kudera, S.; Cingolani, R.; Krahne, R.; Manna, L., Synthesis and Micrometer-Scale Assembly of Colloidal CdSe/CdS Nanorods Prepared by a Seeded Growth Approach. *Nano Lett.* **2007,** 7, 2942-2950.
34. Owen, J. S.; Park, J.; Trudeau, P. E.; Alivisatos, A. P., Reaction chemistry and ligand exchange at cadmium-selenide nanocrystal surfaces. *J. Am. Chem. Soc.* **2008,** 130, 12279-12280.
35. Green, M., The nature of quantum dot capping ligands. *J. Mater. Chem.* **2010,** 20, 5797-5809.
36. Jiang, Z.-J.; Leppert, V.; Kelley, D. F., Static and Dynamic Emission Quenching in Core/Shell Nanorod Quantum Dots with Hole Acceptors. *J. Phys. Chem. C* **2009,** 113, 19161-19171.
37. Rechberger, F.; Heiligtag, F. J.; Süess, M. J.; Niederberger, M., Assembly of BaTiO3 Nanocrystals into Macroscopic Aerogel Monoliths with High Surface Area. *Angew. Chem., Int. Ed.* **2014,** 53, 6823-6826.
38. Wei, H.; Insin, N.; Lee, J.; Han, H.-S.; Cordero, J. M.; Liu, W.; Bawendi, M. G., Compact Zwitterion-Coated Iron Oxide Nanoparticles for Biological Applications. *Nano Lett.* **2012,** 12, 22-25.
39. Etschel, S. H.; Tykwinski, R. R.; Halik, M., Enhancing the Dispersibility of TiO2 Nanorods and Gaining Control over Region-Selective Layer Formation. *Langmuir* **2016,** 32, 10604-10609.
40. De Roo, J.; Yazdani, N.; Drijvers, E.; Lauria, A.; Maes, J.; Owen, J. S.; Van Driessche, I.; Niederberger, M.; Wood, V.; Martins, J. C.; Infante, I.; Hens, Z., Probing Solvent–Ligand

Interactions in Colloidal Nanocrystals by the NMR Line Broadening. *Chem. Mater.* **2018,** 30, 5485-5492.
41. Michaelis, A.; Kaehne, R., Ueber das Verhalten der Jodalkyle gegen die sogen. Phosphorigsäureester oder O-Phosphine. *Ber. Dtsch. Chem. Ges.* **1898,** 31, 1048-1055.
42. Okada, Y.; Ishikawa, K.; Maeta, N.; Kamiya, H., Understanding the Colloidal Stability of Nanoparticle–Ligand Complexes: Design, Synthesis, and Structure–Function Relationship Studies of Amphiphilic Small-Molecule Ligands. *Chem. - Eur. J.* **2018,** 24, 1853-1858.
43. Bhattacharya, A. K.; Thyagarajan, G., Michaelis-Arbuzov rearrangement. *Chem. Rev.* **1981,** 81, 415-430.
44. Kedrowski, S. M. A.; Dougherty, D. A., Room-Temperature Alternative to the Arbuzov Reaction: The Reductive Deoxygenation of Acyl Phosphonates. *Org. Lett.* **2010,** 12, 3990-3993.
45. Rajeshwaran, G. G.; Nandakumar, M.; Sureshbabu, R.; Mohanakrishnan, A. K., Lewis Acid-Mediated Michaelis−Arbuzov Reaction at Room Temperature: A Facile Preparation of Arylmethyl/Heteroarylmethyl Phosphonates. *Org. Lett.* **2011,** 13, 1270-1273.
46. Cohen, R. J.; Fox, D. L.; Eubank, J. F.; Salvatore, R. N., Mild and efficient Cs2CO3-promoted synthesis of phosphonates. *Tetrahedron Lett.* **2003,** 44, 8617-8621.
47. André, V.; Lahrache, H.; Robin, S.; Rousseau, G., Reaction of unsaturated phosphonate monoesters with bromo- and iodo(bis-collidine) hexafluorophosphates. *Tetrahedron* **2007,** 63, 10059-10066.
48. Kosolapoff, G. M., Isomerization of Alkylphosphites. III. The Synthesis of n-Alkylphosphonic Acids. *J. Am. Chem. Soc.* **1945,** 67, 1180-1182.
49. Huang, T.; Chen, T.; Han, L.-B., Oxidative Dephosphorylation of Benzylic Phosphonates with Dioxygen Generating Symmetrical trans-Stilbenes. *J. Org. Chem.* **2018,** 83, 2959-2965.
50. Appel, R., Tertiary Phosphane/Tetrachloromethane, a Versatile Reagent for Chlorination, Dehydration, and P-N Linkage. *Angew. Chem., Int. Ed. Engl.* **1975,** 14, 801-811.
51. M. Crawforth, J.; Fawcett, J.; J. Rawlings, B., Asymmetric synthesis of A-factor. *J. Chem. Soc., Perkin Trans. 1* **1998**, 1721-1726.
52. McKenna, C. E.; Higa, M. T.; Cheung, N. H.; McKenna, M.-C., The facile dealkylation of phosphonic acid dialkyl esters by bromotrimethylsilane. *Tetrahedron Lett.* **1977,** 18, 155-158.
53. Chen, O.; Chen, X.; Yang, Y.; Lynch, J.; Wu, H.; Zhuang, J.; Cao, Y. C., Synthesis of Metal–Selenide Nanocrystals Using Selenium Dioxide as the Selenium Precursor. *Angew. Chem., Int. Ed.* **2008,** 47, 8638-8641.
54. De Roo, J.; Coucke, S.; Rijckaert, H.; De Keukeleere, K.; Sinnaeve, D.; Hens, Z.; Martins, J. C.; Van Driessche, I., Amino Acid-Based Stabilization of Oxide Nanocrystals in Polar Media: From Insight in Ligand Exchange to Solution 1H NMR Probing of Short-Chained Adsorbates. *Langmuir* **2016,** 32, 1962-1970.
55. Lauria, A.; Villa, I.; Fasoli, M.; Niederberger, M.; Vedda, A., Multifunctional Role of Rare Earth Doping in Optical Materials: Nonaqueous Sol–Gel Synthesis of Stabilized Cubic HfO2 Luminescent Nanoparticles. *Acs Nano* **2013,** 7, 7041-7052.
56. Robertson, J., High dielectric constant oxides. *Eur. Phys. J. Appl. Phys.* **2004,** 28, 265-291.
57. Kumar, S.; Wang, Z.; Huang, X.; Kumari, N.; Davila, N.; Strachan, J. P.; Vine, D.; Kilcoyne, A. L.; Nishi, Y.; Williams, R. S., Conduction Channel Formation and Dissolution Due to Oxygen Thermophoresis/Diffusion in Hafnium Oxide Memristors. *ACS Nano* **2016,** 10, 11205-11210.

TOC graphic

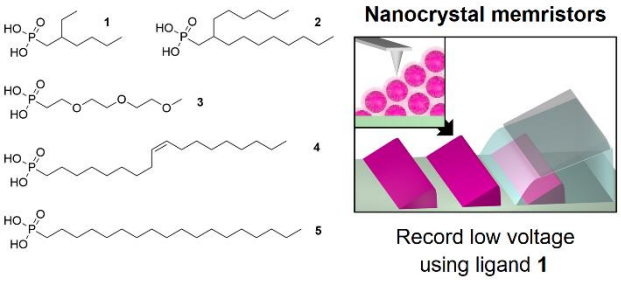
1
2
3
4
5
Nanocrystal memristors
Record low voltage
using ligand 1